Obtaining Large Columnar CdTe Grains and Long Lifetime on Nanocrystalline CdSe, MgZnO, or CdS Layers

Mahisha Amarasinghe, Eric Colegrove, John Moseley, Helio Moutinho, David Albin, Joel Duenow, Soren Jensen, Jason Kephart, Walajabad Sampath, Siva Sivananthan, Mowafak Al-Jassim, and Wyatt K. Metzger**

CdTe solar cells have reached efficiencies comparable to multicrystalline silicon and produce electricity at costs competitive with traditional energy sources. Recent efficiency gains have come partly from shifting from the traditional CdS window layer to new materials such as CdSe and MgZnO, yet substantial headroom still exists to improve performance. Thin film technologies including $Cu(In,Ga)Se_2$, perovskites, $Cu_2ZnSn(S,Se)_4$, and CdTe inherently have many grain boundaries that can form recombination centers and impede carrier transport; however, grain boundary engineering has been difficult and not practical. In this work, it is demonstrated that wide columnar grains reaching through the entire CdTe layer can be achieved by aggressive postdeposition CdTe recrystallization. This reduces the grain structure constraints imposed by nucleation on nanocrystalline window layers and enables diverse window layers to be selected for other properties critical for electro-optical applications. Computational simulations indicate that increasing grain size from 1 to 7 µm can be equivalent to decreasing grain-boundary recombination velocity by three orders of magnitude. Here, large high-quality grains enable CdTe lifetimes exceeding 50 ns.

1. Introduction

Thin-film solar cells are providing electricity at similar costs to conventional sources and can be improved further.[1] Unlike silicon technologies, the active material layer is deposited quickly onto glass, metal, or plastic substrates. This distinction opens up new lightweight and flexible applications as well as paths to substantially lower energy costs in the future; but it also poses fundamental material challenges. The primary photoconversion material is deposited on underlying amorphous or nanocrystalline layers. These window layers can critically affect key material properties such as grain morphology, interface, bulk, grain-boundary (GB) recombination, chemical interdiffusion, and electro-optical properties of the aggregate device. Consequently, a key challenge is to achieve rapid deposition of high quality electro-optical material on nonideal substrates for efficient low-cost solar energy.

CdTe solar cells have improved dramatically in the past 5 years, with cell and module efficiencies reaching 22.1% and 18.6%, respectively.[2,3] This progress has emerged in large part from reexamining the CdS layer in the traditional glass/transparent conducting oxide (TCO)/CdS/CdTe superstrate structure, where the TCO is typically fluorinated SnO_2 but can be other transparent conducting oxides. Early performance improvements were made by incorporating more oxygen in CdS and thinning the layer to reduce absorption.[4–6] Recent research has shifted to replacing the traditional CdS window layer. $Mg_xZn_{1-x}O$ (MZO) is a promising alternative window layer material that has a higher bandgap and has contributed to >18% laboratory cell efficiencies.[7,8] Cadmium selenide (CdSe) is another option; it has been used to adjust bulk lifetime and manipulate absorber bandgap grading to improve photocurrent.[9–12] Because these are novel approaches, publications related to CdSe and MZO in CdTe-based devices are scarce, and there is little knowledge on how these alternate window materials affect nucleation, grain size, and recombination.

Future substantive efficiency gains require overcoming fundamental material issues that have limited open-circuit voltage (V_{OC}) to about 850 mV for decades to realize potential values exceeding 1000 mV.[13,14] This is not trivial because it requires improving both lifetime (including GB, interface, and grain-interior (GI) recombination) and hole density in typical CdTe solar cells by several orders of magnitude.[13,14] A number of studies report that GBs can enhance device performance based on historically poor performance of single-crystal devices, the observation of electrostatic GB potentials, and enhanced electron-beam induced current at GBs.[15–18] However, traditional film stacks built around single-crystal CdTe have overcome historic voltage barriers, and a number of recent studies indicate

M. Amarasinghe, Prof. S. Sivananthan
Department of Physics
University of Illinois at Chicago
Chicago, IL 60607, USA
E-mail: Mahisha.Amarasinghe@nrel.gov

Dr. E. Colegrove, Dr. J. Moseley, Dr. H. Moutinho, Dr. D. Albin, Dr. J. Duenow, Dr. S. Jensen, Dr. M. Al-Jassim, Dr. W. K. Metzger
National Renewable Energy Laboratory
Golden, CO 80401, USA
E-mail: Wyatt.Metzger@nrel.gov

Dr. J. Kephart, Prof. W. Sampath
Department of Mechanical Engineering
Colorado State University
Fort Collins, CO 80523, USA

DOI: 10.1002/aenm.201702666

that GBs are recombination centers.[14,19–25] In polycrystalline solar cells, carrier lifetime correlates well with V_{OC}.[26–29] Therefore, one approach to improve V_{OC} is to increase lifetime by passivating GBs and/or decreasing their density. Recent work demonstrated that lifetime increases with the grain size of as-deposited polycrystalline CdTe;[30] there are no studies that clearly indicate a relationship between grain size and lifetime of polycrystalline CdTe in standard $CdCl_2$-treated solar cells. Earlier detailed electron backscatter diffraction (EBSD) studies have shown that as-deposited films generally have small grains near the nanocrystalline interface and these small grains can coalescence with depth during growth.[31–33] When films or regions start with grain diameter less than 1 µm, including films deposited near room temperature by sputtering or electrodeposition, recrystallization has often been observed to enhance grain size. For films or regions with larger as-deposited grains, typically achieved at higher substrate temperatures by methods such as close-spaced sublimation (CSS) and physical vapor deposition, the grain size was not enhanced with recrystallization in earlier work.[31–33] Most reported studies have not explored $CdCl_2$ temperatures beyond about 425 °C. In part, this is because it has been difficult to significantly manipulate grain size for thin films deposited on glass and nanocrystalline layers such as TCOs and CdS without incurring deleterious stress and delamination.

In this work, we examine how CdTe grain size and carrier lifetime can be increased over a range of $CdCl_2$ temperatures with different window layers—CdS, CdSe, and MZO. Time-correlated single-photon counting and cathodoluminescence (CL) indicate the mechanisms that initially decrease and then increase recombination during grain growth. Computational models indicate the degree to which large grains can help reduce recombination and provide upper-limit estimates for GB and surface recombination. We find that the initial absorber nucleation is not critical. By carefully manipulating the recrystallization process, different window materials can support high-quality large-grain CdTe thin films with minimal horizontal GBs and excellent lifetimes.

2. Results and Discussion

Figure 1 illustrates the sample structures of alternative window layer/CdTe devices. Consistent with manufacturable processes, CdS, CdSe, and MZO were sputtered at room temperature on SnO_2:F coated glass to form the underlying substrate. CdTe was then deposited at substrate temperatures of 600 °C using CSS

Figure 1. Device structures of the fabricated CdS/CdTe, CdSe/CdTe, and MZO/CdTe devices.

on each window layer.[34,35] The experimental section describes the processes and measurements in detail. Vapor $CdCl_2$ treatments were conducted at temperatures ranging from 400 to 490 °C in a CSS chamber for 10 min in an oxygen-containing ambient.

During this process, Cl diffuses rapidly along GBs as well as throughout the CdTe film and window layers.[36–38] The process allows bonds to break and reform, with end defect chemistries and reactions driven in part by ambient elements.[39] The presence of oxygen can draw Cd to the surface, cause GBs to form oxide compounds, and adjust GB electronic and chemical properties.[39,40] At the same time, S or Se, if present in the window layer, generally interdiffuse with the CdTe to form an alloy at the interface and this has been linked to reduced recombination.[10,41–45] Overall the $CdCl_2$ effects can cause significant stress, and partially or completely consume layers in the film stack. As a result, increasing the $CdCl_2$ temperature has frequently caused severe adhesion and delamination issues. Different window layers may provide different results. By sustaining a higher substrate temperature than the $CdCl_2$ source here, the formation of discrete layers of $CdCl_2$ or oxychlorides is reduced. These layers can weaken the interfacial adhesion of CdTe and window layers to the transparent conducting oxide partly from different coefficients of thermal expansion. This approach helps maintain film integrity while allowing the exploration of recrystallization properties at temperatures well above 400 °C.

The grain size at the back of the film was measured using EBSD and optical microscopy imaging, which were in good agreement. The latter are presented in Figure S1 of the Supporting Information. The CdTe grain structure from the window/CdTe interface to the back of the film was profiled by cross-sectional EBSD. Historically films deposited at 600 °C by CSS produce large as-deposited grains relative to other methods and/or lower temperature depositions, and it was reported that $CdCl_2$ treatments failed to enhance these larger grains.[32,33] Here, we examine if different window layers combined with aggressive recrystallization can facilitate engineering novel grain structures with enhanced carrier lifetime and transport properties.[21]

Figure 2 illustrates the different orientations normal to the CdTe surface in planar EBSD images for CdTe on CdS, CdSe, and MZO. Here, as-deposited CdTe on CdS is randomly oriented, whereas as-deposited CdTe on CdSe and MZO show weak and stronger preferential orientations along the (111) plane respectively. After the $CdCl_2$ treatment, CdTe has no preferential orientation and the grains are larger than as-deposited CdTe, indicating recrystallization driving grain growth.

The cross-sectional EBSD images of CdTe on CdS and MZO in **Figure 3** indicate that grain growth occurs throughout the CdTe film. Results for CdSe (not shown) are very similar to CdS. Corresponding inverse pole figure maps showing orientation normal to the cross-section of CSS CdTe are given in Figure S2 in the Supporting Information. For as-deposited and low-temperature $CdCl_2$ treatments, clusters of smaller grains are observed at the window/CdTe interface. This GB density can increase recombination in the critical junction region. At higher $CdCl_2$ temperatures, these small grains near the interface are mostly eliminated, and columnar grains extend uninterrupted from the interface to the back of the CdTe film, which reduces carrier transport across GBs. $CdCl_2$ treatment steadily

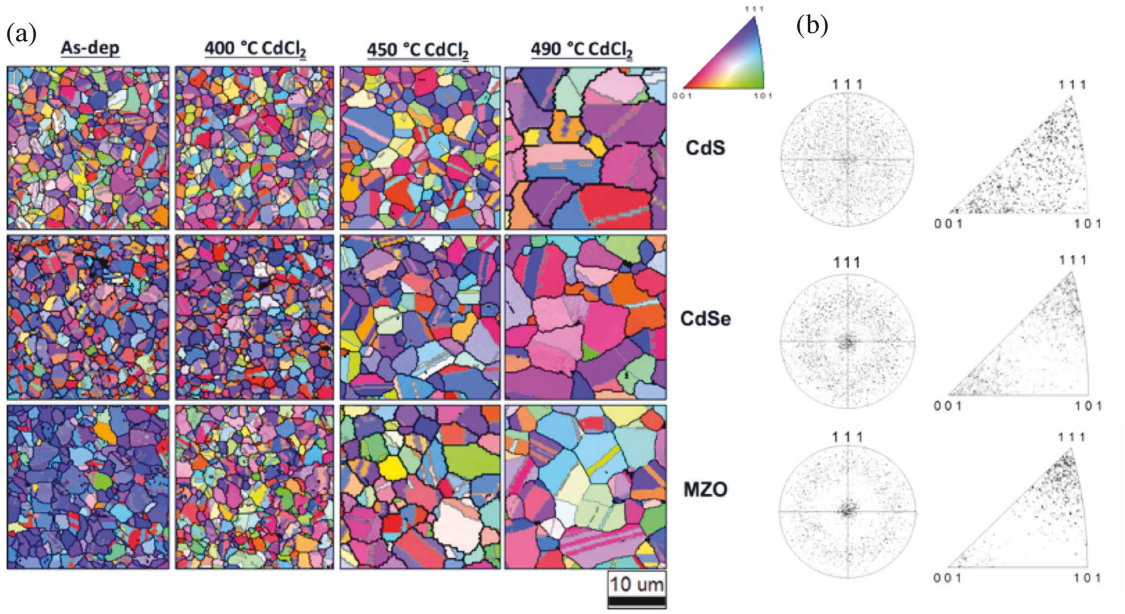

Figure 2. a) Planar EBSD inverse pole figure maps showing orientation normal to the surface of CSS CdTe deposited on (top to bottom) CdS, CdSe, and MZO for (left to right) as-deposited films and 400, 450, and 490 °C $CdCl_2$ temperatures. Σ3 boundaries are gray and other GBs are black. b) (111) pole figures and inverse pole figures of as-deposited CdTe on (top to bottom) CdS, CdSe, and MZO.

increases grain size while eliminating smaller interface grains in devices up to about 450 °C. However, at 490 °C, the grains begin to separate, forming voids.

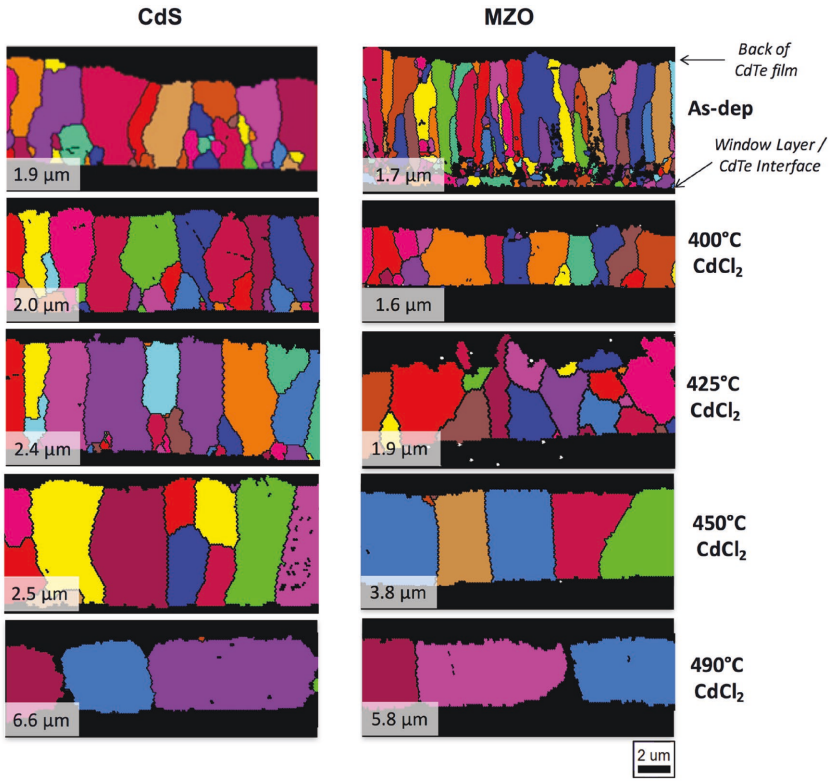

Figure 3. Cross-sectional EBSD grain maps of CSS CdTe deposited on (left to right) CdS and MZO for (top to bottom) as-deposited films and 400, 425, 450, and 490 °C $CdCl_2$ temperatures. Black lines are GBs and average grain size is reported in the bottom left.

Figure 4 plots the average grain size as a function of $CdCl_2$ temperature for CdTe on CdS, CdSe, and MZO. The grain size clearly increases steadily with $CdCl_2$ temperature. Furthermore, the trends are similar among the different window layers. These data indicate that the recrystallization can rectify initial differences in film orientation and nucleation from different window layers while enhancing grain size and structure.

Carrier lifetimes were measured by exciting luminescence through the glass with 640 nm laser excitation from 0.3 ps pulses and generating photoluminescence (PL) decay curves by time-correlated single-photon counting. Time-dependent differential equations for Poisson and electron and hole continuity equations were solved by Sentaurus software to simulate and interpret the time-resolved experiments and characterize how GB recombination affects lifetime for different grain sizes.[46] The simulations were matched to the experimental pulse duration and photoinjection levels. Because the light is largely absorbed in the CdTe/window p–n junction depletion region, high-injection conditions screen the field and charge separation effects.[47] The modeling indicates that just 1–2 ns after the laser pulse, for the experimental injection levels chosen here, the PL decay curves represent recombination as if the junction were not present.[29,47–50] Consequently, lifetimes were taken from the latter section of the decay curve using biexponential decay

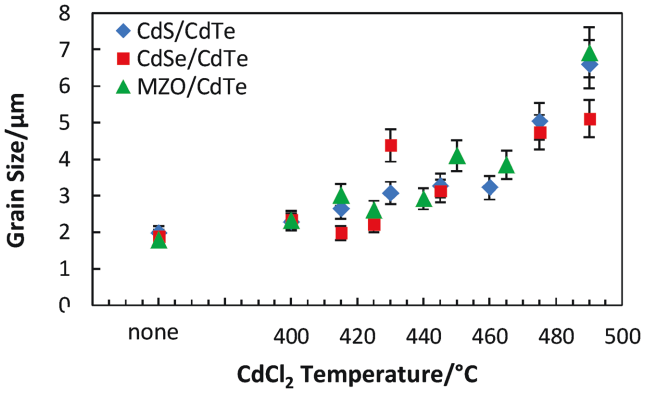

Figure 4. Grain size determined from optical microscopy on the CdTe back surface versus $CdCl_2$ temperature for CSS CdTe on CdS, CdSe, and MZO.

fits as shown in an example in Figure S3 in the Supporting Information.

Figure 5 indicates the room temperature lifetimes as a function of grain size and nucleation layer. The error for these lifetimes is ≈±10%. For CdS, CdSe, and MZO, the interface recombination is sufficiently low to enable lifetimes above 10 ns. S and Se are known to diffuse readily across the interface into the CdTe absorber layer, particularly along the GBs during the $CdCl_2$ treatment.[10,44,45] The favorable results for CdS, CdSe, and MZO indicate that S or Se interdiffusion is not critical to achieve lifetimes of tens of nanoseconds. For the different window layers, lifetimes reach maximum values from 20 to 60 ns at $CdCl_2$ temperatures between 445 and 465 °C before flattening or declining with increasing temperature.

The as-deposited CdTe data given by black squares are extracted from earlier work examining small- and large-grain thick polycrystalline CdTe films deposited on Mo without $CdCl_2$, using two-photon excitation to measure lifetime.[30] Given the experimental differences, the results for thin as-deposited CdTe on CdS, CdSe, and MZO indicated by open colored markers in Figure 5 align with this earlier study reasonably well. For

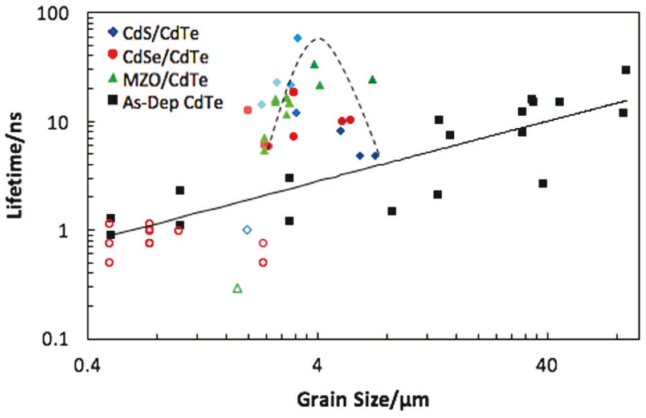

Figure 5. Lifetime versus grain size data for CdTe on CdS, CdSe, and MZO coupled with non-$CdCl_2$-treated CdTe data from ref. [30] (black symbols). As-deposited CdTe on CdS, CdSe, and MZO are indicated with open markers, and darker shades indicate higher $CdCl_2$ temperatures. The black dashed curve shows the general trend of $CdCl_2$-treated samples.

$CdCl_2$-treated samples, the lifetime increases more quickly with grain size and enables higher lifetimes for a given grain size. As the $CdCl_2$ temperature increases beyond 460 °C, lifetime begins to flatten or decrease with increasing grain size.

A number of factors can adjust recombination. $CdCl_2$ treatments are reported to influence lifetime by GB defect passivation and intragrain defect reduction.[23–25,33,51–54] To understand the mechanisms driving these lifetime changes, we conducted CL measurements, which have the spatial resolution (100 nm) to assess GB and intragrain recombination. The gray scale in the CL images is normalized to the maximum and minimum integrated spectral intensity in each image.

Figure 6 indicates the CL intensity as a function of position for as-deposited films and $CdCl_2$ temperatures of 415, 440, 465, and 490 °C on MZO. The darker regions in the CL images indicate less luminescence. Because the injection levels are high relative to the equilibrium hole density and the samples are polished, less luminescence is driven by higher recombination rates. The data indicate that there are multiple mechanisms that are improving lifetime with increasing temperature. In addition to the grain size increasing, the intragrain quality steadily improves. At 465 °C, very large high-quality grains are observed. With increasing grain size, the lifetime increases and we would expect that if the GB recombination velocity were constant, the CL intensity at the GBs would decrease relative to the grain interior. Instead, we observe the opposite trend with increasing $CdCl_2$ temperature, indicating that the GBs are increasingly, but not completely, passivated up to 465 °C. However, at 465 °C, small voids start to occur at triple points. At higher temperatures, the grains begin to segregate from one another and create significant recombination. Corresponding scanning electron microscope (SEM) images on the same samples in **Figure 7** show this grain segregation clearly.

Models simulating time-resolved photoluminescence (TRPL) measurements on complete devices with TCO/CdS/CdTe layers and columnar grains as shown in **Figure 8** were executed for different grain sizes, intragrain bulk lifetimes (τ_{bulk}), CdTe/window interface recombination velocities (S), and GB recombination velocities (S_{gb}) using standard material parameters described in the Experimental Section and the Supporting Information.

Figure 9 shows TRPL decays where S and τ_{bulk} are set to 0 cm s^{-1} and 500 ns, respectively, whereas different curve colors represent S_{gb} ranging from 0 to 10^7 cm s^{-1}. The total recombination rate is given by the sum of grain interior, GB, and interfacial recombination, thus by choosing a long bulk lifetime of 500 ns, and setting interface recombination to zero, we can establish the upper limits for GB recombination. Interestingly, the simulation results demonstrate that 500 ns bulk lifetimes can be observed for the experimental injection levels here, despite the presence of a junction. Common intuition is that GBs and surface recombination will generally affect the initial decay and that the final decay will represent longer intragrain lifetimes; however, it is incorrect to assume that the final decay necessarily represents longer grain interior recombination. Here we observe that even though the intragrain lifetime is as high as 500 ns, this long lifetime will generally not be observed for even moderate GB recombination velocities. So, it is possible that GB and/or interface recombination can dominate the entire decay curve and often drive the lifetimes that the thin-film

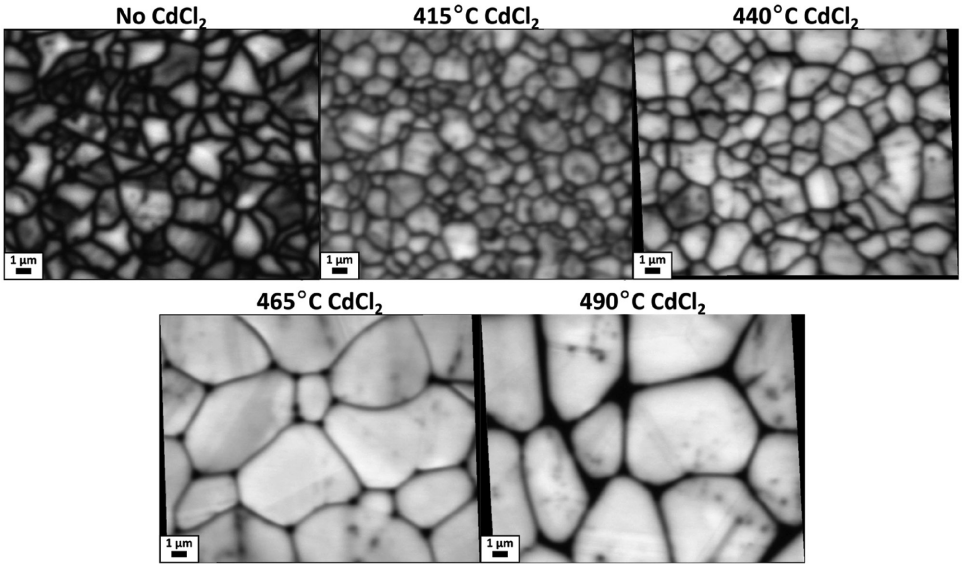

Figure 6. CL images of as-deposited and $CdCl_2$-treated CdTe films deposited on MZO.

community measures in practice. Furthermore, Figure 9 illustrates that as grain size is increased from 1 to 7 µm, effective GB recombination can be reduced by orders of magnitude. For example, a film with 7 µm grains and $S_{gb} = 10^7$ cm s^{-1} has a comparable lifetime to 1 µm grains with $S_{gb} = 10^4$ cm s^{-1}.

Figure 10 shows the calculated lifetime values from exponential fits of the latter section of the simulated decay curves for $\tau_{bulk} = 500$ ns with S (x-axis) and S_{gb} (curve colors) ranging from 0 to 10^7 cm s^{-1}. The lifetime range naturally decreases when the CdTe/window interface recombination increases, particularly for $S \geq 10^5$ cm s^{-1}. The modeling indicates the combinations of grain size, interface recombination, and GB recombination velocities that are required to achieve lifetimes exceeding 10 and 100 ns assuming minimal bulk recombination. We estimate upper limits for S_{gb} by assuming minimal intragrain (500 ns) and interface recombination (0 cm s^{-1}), and an upper bound of S by assuming S_{gb} is 0 cm s^{-1} and 500 ns intragrain lifetime. For 3 µm films to achieve 10 ns lifetimes that are frequently measured here, S_{gb} must be $<2.5 \times 10^4$ cm s^{-1} and interface recombination $S < 10^5$ cm s^{-1}. To approach the measured value of 60 ns, S_{gb} and S must be less than 10^4 cm s^{-1}. This is an order of magnitude less than measurements on a range of polycrystalline CdTe films, where S and S_{gb} were estimated to be $>10^5$ cm s^{-1}.[23,25,55,56]

S and Se alloying can adjust the bandgap, bandgap grading, as well as interface quality. Impurity diffusion can vary with grain size, and doping and optimum back contact preparation may vary with $CdCl_2$ temperature. These and other variables can influence V_{oc}, fill factor, photocurrent, and efficiency; so complete optimization for each condition is required for a fair comparison and beyond the scope of this work. For optimization on MZO, the reported grain size and lifetime improvements here have been critical to increasing laboratory cell efficiency beyond 19%.[57]

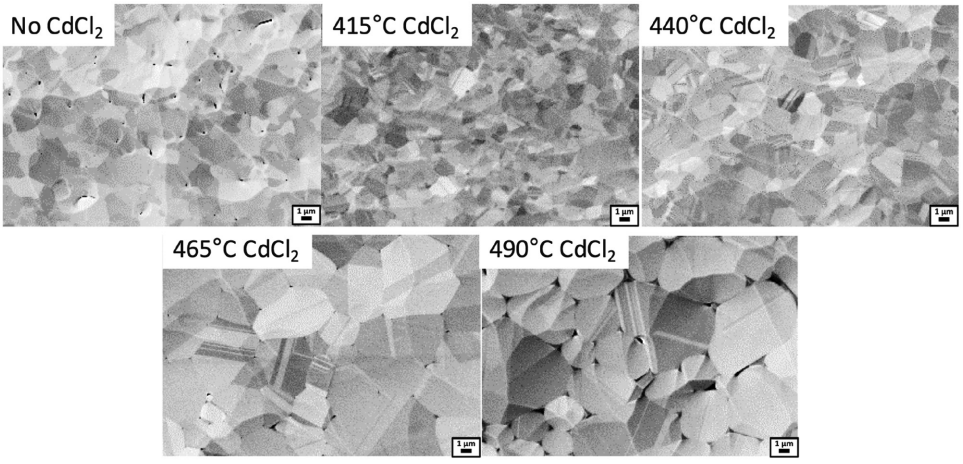

Figure 7. SEM images of as-deposited and $CdCl_2$-treated CdTe films deposited on MZO.

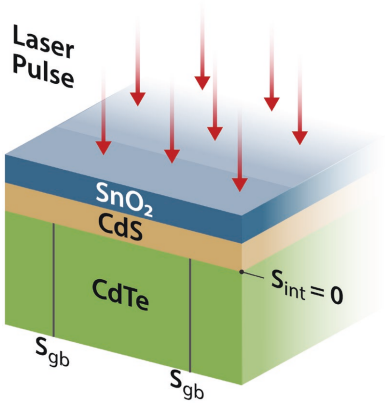

Figure 8. Device structure used for models simulating TRPL decay curves.

3. Conclusion

Simulations indicate that increasing grain size from 1 to 7 µm can be equivalent to reducing S_{gb} by three orders of magnitude. In practice, increasing the $CdCl_2$-treatment temperature enables enhancing the grain size by recrystallizing polycrystalline CdTe films on CdSe, MZO, or CdS window layers. The lifetime increases with grain size prior to grains separating from one another, with a more abrupt slope for $CdCl_2$-treated samples than as-deposited samples. This is consistent with partial but not complete passivation of GBs by the $CdCl_2$ treatment. The results indicate that S and Se interdiffusion are not critical to achieve lifetimes greater than 10 ns. Different window layers can be used to form high-quality large-grain CdTe thin films. For decades, the thin film CdTe community has had relatively little control of grain structure and poor understanding of its relation with lifetime. In this work, we show that aggressive postdeposition recrystallization can be coupled with various window layers to achieve wide columnar grains reaching through the entire CdTe layer. This reduces the grain structure constraints imposed by high throughput deposition on nanocrystalline window layers and enables diverse window layers to be selected for other properties critical for electro-optical applications. At the same time, long lifetimes can be achieved to overcome longstanding material limits and enable high-performance solar cells.

4. Experimental Section

CdS and CdSe were deposited at room temperature on SnO_2:F-coated Corning 7059 glass in a Lesker CMS-18 radio-frequency (RF) planar sputtering system. About 80 nm of CdS was deposited from a 99.99%-pure target at 5 mTorr of 6% flowing oxygen in argon using a power of 100 W. In distinct synthesis, 150 nm of CdSe was deposited from a 99.995%-pure target at 5 mTorr of 100% flowing argon using a power of 100 W. MZO films were also deposited by RF planar magnetron sputter deposition, but on SnO_2:F-coated soda-lime glass. The 100 nm films were deposited from a mixed-oxide target with a composition of 11 wt% MgO/89 wt% ZnO and 99.99% purity at 5 mTorr of 3% flowing oxygen in argon using a power of 180 W.

CdTe was deposited at a substrate temperature of 600 °C using CSS on each window layer.[34,35] Vapor $CdCl_2$ treatments were conducted at temperatures ranging from 400 to 490 °C in a CSS chamber for 10 min in an oxygen-containing ambient. Temperatures during sample deposition and $CdCl_2$ treatment were monitored continuously by thermocouples embedded in graphite susceptors supporting the samples and source material. While the glass surface temperature is not measured directly, it is expected to be within 5 °C of the monitored graphite temperature. The $CdCl_2$ substrate temperature was held 5 °C above the source temperature.

Bright-field optical microscopy images were obtained using a Zeiss M2m Imager with AxioVision software at 100× magnification. A Benson etch[58] was performed to observe the GBs clearly by optical microscopy. The EBSD analysis was performed in SEM FEI Nova 630 NanoSEM using an EDAX Pegasus/Hikari A40 system. To avoid shading effects due to the roughness of the surface and cross section, the samples were ion milled in a JEOL cross-section polisher. The grain size determination

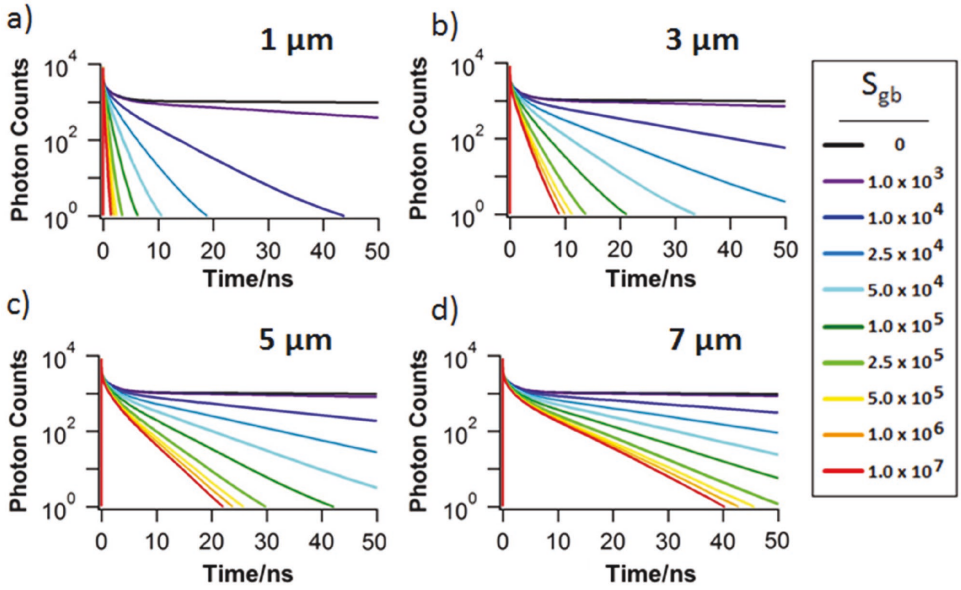

Figure 9. Simulated TRPL decays for τ_{bulk} = 500 ns and S = 0 for a) 1 µm, b) 3 µm, c) 5 µm, and d) 7 µm grains and different GB recombination velocities (S_{gb}).

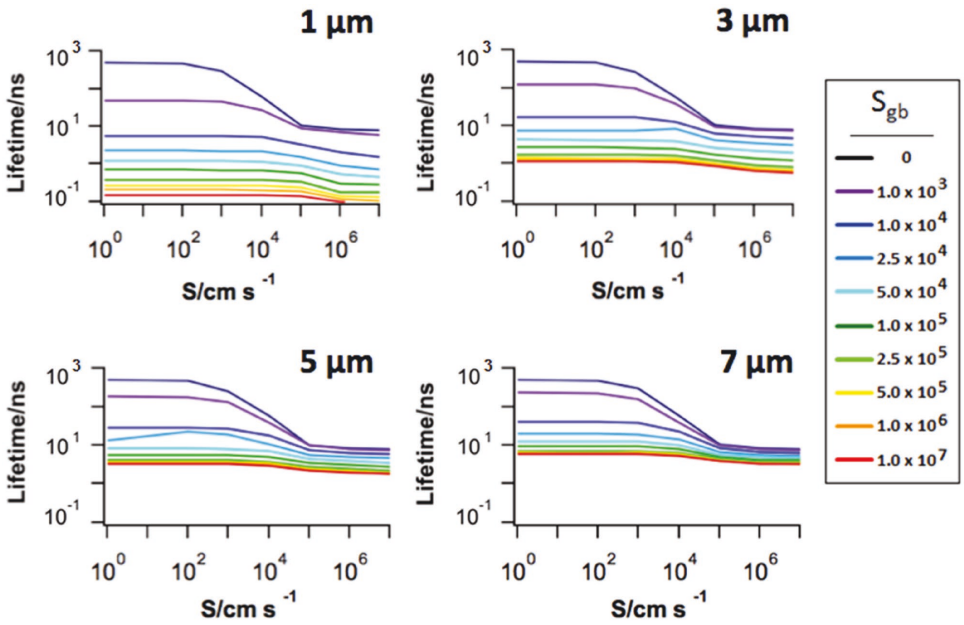

Figure 10. Lifetime versus S for CdTe grain sizes of 1, 3, 5, and 7 µm and a range of S_{gb} values.

method by optical microscopy used the American Society for Testing and Materials (ASTM) Standard E112-12[59] and produced similar results to the numerical average grain size determined by analysis algorithms in the EBSD software.

For TRPL measurements, laser pulses 300 ps in temporal width were fired at a rate of 1.1 MHz and focused to an approximate spot size of 300 µm with aggregate average (CW) power of about 200 µW. A dichroic beamsplitter separated collinear laser excitation from luminescence. A microphoton devices silicon avalanche photodiode detector was used for single-photon detection for photons passed through Thorlab interference filters with 10 nm bandwidth and 840 nm center wavelengths. Time-correlated single-photon counting is used to generate decay curves with high temporal resolution and linear dynamic response. After deconvolution with the instrument system response, 20 ps lifetimes can be resolved.

Computational simulations were performed using Sentaurus Device software[46] to solve the Poisson and electron and hole continuity equations. The model device consisted of three semiconductor layers: SnO_2, CdS, and CdTe. The principal properties for each layer are provided in Table S1 in the Supporting Information. In lieu of traps, the electron and hole lifetimes were input as 100 and 10 ps in the SnO_2 and CdS, respectively. The input electron densities in SnO_2 and CdS were 10^{18} and 10^{15} cm^{-3}, respectively, and hole density in CdTe was 2×10^{14} cm^{-3}. Simulation results presented here are not sensitive to variations in these parameters. Columnar CdTe GBs were modeled with two GBs separated by the grain size and half the grain size to the lateral edges of the model for periodicity and are shown in Figure 8. The model inserts the electron and hole lifetimes into the Shockley–Read–Hall recombination equation.[46] The electron and hole lifetimes were set equal. This approach reproduces both time-resolved photoluminescence measurements and experimental lifetime and V_{OC} correlations.[26,28,29,60] Lifetime values in the simulations were determined with exponential decay fits as in the experiments. The thermal velocity was approximated as 10^7 $cm\,s^{-1}$.

Prior to CL, samples were ion milled flat using an Ar^+ ion beam in a JEOL Cross-Section Polisher. Samples were tilted at a 5° glancing angle to a 4 kV ion beam and milled for 30–50 min to remove the surface roughness. Our previous work has shown that this type of ion milling does not significantly affect the peaks in low-temperature CdTe luminescence spectra.[61] More recently, 1PE TRPL was conducted on Ar^+ ion-milled surfaces and it was determined that the surface recombination velocity was about the same as for samples that were not ion milled, ≈10^5 cm s^{-1}.[62]

CL spectrum imaging measurements were performed at room temperature on a JEOL 7600F field-emission SEM equipped with a Horiba H-cathodoluminescence universal extension (CLUE) CL system. The e-beam voltage and current used in CL were 7.5 kV and 6 nA, respectively. With these conditions, the steady-state excess-carrier density is about 10^{17} cm^{-3} directly under the beam in the grain-interior. Luminescence spectra were recorded at each image pixel using an iHR320 spectrometer with a Syncerity charge-coupled device (CCD) detector and a grating with 300 grooves mm^{-1}, blazed to 600 nm.

Supporting Information

Supporting Information is available from the Wiley Online Library or from the author.

Acknowledgements

This work was supported by the U.S. Department of Energy under Contract No. DE-AC36-08GO28308 to the National Renewable Energy Laboratory that covers subcontract XEU-2-22078-01 University of Illinois at Chicago grant# 3323.

Conflict of Interest

The authors declare no conflict of interest.

Keywords

CdTe, grain boundaries, recombination, solar energy, thin films

Received: September 23, 2017
Published online: January 15, 2018

[1] U.S. Energy Information Administration, https://www.eia.gov/outlooks/aeo/pdf/electricity_generation.pdf (accessed: December 2017).
[2] National Renewable Energy Laboratory, https://www.nrel.gov/pv/assets/images/efficiency-chart.png (accessed: December 2017).
[3] M. Green, K. Emery, Y. Hishikawa, W. Warta, E. Dunlop, D. Levi, A. Ho-Baillie, *Prog. Photovoltaics* **2016**, *25*, 3.
[4] X. Wu, *Sol. Energy* **2004**, *77*, 803.
[5] J. Kephart, R. Geisthardt, W. Sampath, *Prog. Photovoltaics* **2015**, *23*, 1484.
[6] D. Meysing, C. Wolden, M. Griffith, H. Mahabaduge, J. Pankow, M. Reese, J. Burst, W. Rance, T. Barnes, *J. Vac. Sci. Technol., A* **2015**, *33*, 021203.
[7] J. Kephart, J. McCamy, Z. Ma, A. Ganjoo, F. Alamgir, W. Sampath, *Sol. Energy Mater. Sol. Cells* **2016**, *157*, 266.
[8] J. Sites, A. Munshi, J. Kephart, D. Swanson, W. Sampath, *IEEE Photovoltaic Spec. Conf., 43rd*, Portland, OR, June **2016**.
[9] M. Gloeckler, *IEEE Photovoltaic Spec. Conf., 43rd*, Portland, OR, June **2016**.
[10] J. D. Poplawsky, W. Guo, N. Paudel, A. Ng, K. More, D. Leonard, Y. Yan, *Nat. Commun.* **2016**, *7*, 12537.
[11] D. Swanson, J. Sites, W. Sampath, *Sol. Energy Mater. Sol. Cells* **2017**, *159*, 389.
[12] A. R. Duggal, J. J. Shiang, W. H. Huber, A. F. Halverson (First Solar Inc.), *US Patent Application 13/923,644*, **2013**.
[13] A. Kanevce, M. Reese, T. Barnes, S. Jensen, W. K. Metzger, *J. Appl. Phys.* **2017**, *121*, 214506.
[14] J. Burst, J. Duenow, D. Albin, E. Colegrove, M. Reese, J. Aguiar, C. Jiang, M. Patel, M. M. Al-Jassim, D. Kuciauskas, S. Swain, T. Ablekim, K. Lynn, W. K. Metzger, *Nat. Energy* **2016**, *1*, 16015.
[15] I. Visoly-Fisher, S. Cohen, A. Ruzin, D. Cahen, *Adv. Mater.* **2004**, *16*, 879.
[16] Y. Yan, W. Yin, Y. Wu, T. Shi, N. Paudel, C. Li, J. Poplawsky, Z. Wang, J. Moseley, H. Guthrey, H. R. Moutinho, S. J. Pennycook, M. M. Al-Jassim, *J. Appl. Phys.* **2015**, *117*, 112807.
[17] C. Li, Y. Wu, J. Poplawsky, T. J. Pennycook, N. Paudel, W. Yin, S. Haigh, M. Oxley, A. Lupini, M. M. Al-Jassim, S. J. Pennycook, Y. Yan, *Phys. Rev. Lett.* **2014**, *112*, 156103.
[18] J. Poplawsky, N. Paudel, C. Li, C. Parish, D. Leonard, Y. Yan, S. J. Pennycook, *Adv. Energy Mater.* **2014**, *4*, 1400454.
[19] J. Moseley, W. K. Metzger, H. R. Moutinho, N. Paudel, H. Guthrey, Y. Yan, R. Ahrenkiel, M. M. Al-Jassim, *J. Appl. Phys.* **2015**, *118*, 025702.
[20] J. Moseley, M. M. Al-Jassim, H. Guthrey, J. Burst, J. Duenow, R. Ahrenkiel, W. K. Metzger, *J. Appl. Phys.* **2016**, *120*, 105704.
[21] G. Stechmann, S. Zaefferer, T. Schwarz, P. Konijnenberg, D. Raabe, C. Gretener, L. Kranz, J. Perrenoud, S. Buecheler, A. Nath Tiwari, *Sol. Energy Mater. Sol. Cells* **2017**, *166*, 108.
[22] W. K. Metzger, M. Gloeckler, *J. Appl. Phys.* **2005**, *98*, 063701.
[23] A. Kanevce, J. Moseley, M. M. Al-Jassim, W. K. Metzger, *IEEE J. Photovoltaics* **2015**, *5*, 1722.
[24] B. Gaury, P. Haney, *J. Appl. Phys.* **2016**, *120*, 234503.
[25] J. Major, *Semicond. Sci. Technol.* **2016**, *31*, 093001.
[26] W. K. Metzger, D. Albin, D. Levi, P. Sheldon, X. Li, B. Keyes, R. Ahrenkiel, *J. Appl. Phys.* **2003**, *94*, 3549.
[27] D. Kuciauskas, P. Dippo, Z. Zhao, L. Cheng, A. Kanevce, W. K. Metzger, M. Gloeckler, *IEEE J. Photovoltaics* **2016**, *6*, 313.
[28] J. Duenow, J. Burst, D. Albin, M. Reese, S. Jensen, S. Johnston, D. Kuciauskas, S. Swain, T. Ablekim, K. Lynn, A. Fahrenbruch, W. K. Metzger, *IEEE J. Photovoltaics* **2016**, *6*, 1641.
[29] W. K. Metzger, M. J. Romero, P. Dippo, M. Young, *IEEE 4th World Conf. Photovoltaic Energy Convers* **2006**, *1*, 372.
[30] S. Jensen, J. Burst, J. Duenow, H. Guthrey, J. Moseley, H. R. Moutinho, S. Johnston, A. Kanevce, M. M. Al-Jassim, W. K. Metzger, *Appl. Phys. Lett.* **2016**, *108*, 263903.
[31] G. Stechmann, S. Zaefferer, P. Konijnenberg, D. Raabe, C. Gretener, L. Kranz, J. Perrenoud, S. Buecheler, A. Tiwari, *Sol. Energy Mater. Sol. Cells* **2016**, *151*, 66.
[32] H. R. Moutinho, R. G. Dhere, M. J. Romero, C. -S. Jiang, B. To, M. M. Al-Jassim, *J. Vac. Sci. Technol., A* **2008**, *26*, 1068.
[33] H. R. Moutinho, R. Dhere, C. Ballif, M. M. Al-Jassim, L. Kazmerski, *J. Vac. Sci. Technol., A* **2000**, *18*, 1599.
[34] T. L. Chu, S. S. Chu, J. Britt, C. Ferekides, C. Wang, C. Q. Wu, H. S. Ullal, *IEEE Electron Device Lett.* **1992**, *13*, 303.
[35] D. H. Rose, F. S. Hasoon, R. G. Dhere, D. S. Albin, R. M. Ribelin, X. S. Li, Y. Mahathongdy, T. A. Gessert, P. Sheldon, *Prog. Photovoltaics* **1999**, *7*, 331.
[36] M. B. Dutt, B. L. Sharma, in *Diffusion in Semiconductors and Non-Metallic Solids* (Ed: D. L. Beke), Springer-Verlag, Berlin **1998**, p. 3–1.
[37] D. Mao, C. E. Wickersham, M. Gloeckler, *IEEE J. Photovoltaics* **2014**, *4*, 1655.
[38] S. Harvey, G. Teeter, H. R. Moutinho, M. M. Al-Jassim, *Prog. Photovoltaics* **2015**, *23*, 838.
[39] B. E. McCandless, S. S. Hegedus, R. W. Birkmire, D. Cunningham, *Thin Solid Films* **2003**, *431*, 249.
[40] B. E. McCandless, *Mater. Res. Soc. Symp. Proc.* **2013**, *1538*, 249.
[41] L. Kranz, C. Gretener, J. Perrenoud, D. Jaeger, S. Gerstl, R. Schmitt, S. Buecheler, A. Tiwari, *Adv. Energy Mater.* **2014**, *4*, 1301400.
[42] W. K. Metzger, D. Albin, M. Romero, P. Dippo, M. Young, *J. Appl. Phys.* **2006**, *99*, 103703.
[43] M. Terheggen, H. Heinrich, G. Kostorz, D. Baetzner, A. Romeo, A. Tiwari, *Interface Sci.* **2004**, *12*, 259.
[44] C. Li, J. Poplawsky, N. Paudel, T. J. Pennycook, S. J. Haigh, M. M. Al-Jassim, Y. Yan, S. J. Pennycook, *IEEE J. Photovoltaics* **2014**, *4*, 1636.
[45] B. McCandless, M. Engelmann, R. Birkmire, *J. Appl. Phys.* **2001**, *89*, 988.
[46] Synopsys, TCAD SDEVICE Manual, Release H-2013.03, Zurich, Switzerland, www.synopsys.com, (accessed: December 2017).
[47] W. K. Metzger, R. K. Ahrenkiel, J. Dashdorj, D. J. Friedman, *Phys. Rev. B* **2005**, *71*, 035301.
[48] M. Maiberg, R. Scheer, *J. Appl. Phys.* **2014**, *116*, 123711.
[49] W. K. Metzger, I. L. Repins, M. A. Contreras, *Appl. Phys. Lett.* **2008**, *93*, 022110.
[50] W. K. Metzger, I. L. Repins, M. Romero, P. Dippo, M. A. Contreras, R. Noufi, D. Levi, *Thin Solid Films* **2009**, *517*, 2360.
[51] E. S. Barnard, B. Ursprung, E. Colegrove, H. R. Moutinho, N. J. Borys, B. E. Hardin, C. H. Peters, W. K. Metzger, P. J. Schuck, *Adv. Mater.* **2017**, *29*, 1603801.
[52] J. D. Major, M. Al Turkestani, L. Bowen, M. Brossard, C. Li, P. Lagoudakis, S. J. Pennycook, L. J. Phillips, R. E. Treharne, K. Durose, *Nat. Commun.* **2016**, *7*, 13231.
[53] I. Dharmadasa, *Coatings* **2014**, *4*, 282.
[54] N. Paudel, M. Young, P. Roland, R. Ellingson, Y. Yan, A. Compaan, *J. Appl. Phys.* **2014**, *115*, 064502.

[55] M. Reese, C. Perkins, J. Burst, S. Farrell, T. Barnes, S. Johnston, D. Kuciauskas, T. Gessert, W. K. Metzger, *J. Appl. Phys.* **2015**, *118*, 155305.
[56] M. Reese, J. Burst, C. Perkins, A. Kanevce, S. Johnston, D. Kuciauskas, T. Barnes, W. K. Metzger, *IEEE J. Photovoltaics* **2015**, *5*, 382.
[57] A. Munshi, J. Kephart, A. Abbas, J. Raguse, J. Beaudry, K. Barth, J. Sites, J. Walls, W. Sampath, *IEEE Photovoltaic Spec. Conf., 44th*, Washington, DC, June **2017**.
[58] Benson, L. Bubulac, P. Smith, R. Jacobs, J. Markunas, M. Jaime-Vasquez, L. Almeida, A. Stoltz, P. Wijewarnasuriya, G. Brill, Y. Chen, U. Lee, M. Vilela, J. Peterson, S. Johnson, D. Lofgreen, D. Rhiger, E. Patten, P. Goetz, *J. Electron. Mater.* **2010**, *39*, 1080.
[59] *ASTM E112-12, Standard Test Methods for Determining Average Grain Size*, ASTM International, West Conshohocken, PA **2012**, https://doi.org/10.1520/E0112-12.
[60] H. Mahabaduge, W. Rance, J. Burst, M. Reese, D. Meysing, C. Wolden, J. Li, J. Beach, T. Gessert, W. K. Metzger, S. Garner, T. Barnes, *Appl. Phys. Lett.* **2015**, *106*, 133501.
[61] J. Moseley, M. M. Al-Jassim, D. Kuciauskas, H. R. Moutinho, N. Paudel, H. L. Guthrey, Y. Yan, W. K. Metzger, R. K. Ahrenkiel, *IEEE J. Photovoltaics* **2014**, *4*, 1671.
[62] J. Moseley, P. Rale, S. Collin, A. Kanevce, E. Colegrove, J. Duenow, S. Jensen, W. K. Metzger, M. M. Al-Jassim, *IEEE Photovoltaic Spec. Conf., 44th*, Washington, DC, June **2017**.